ELSEVIER

Sedimentary Geology 145 (2001) 23–43

Sedimentary Geology

www.elsevier.com/locate/sedgeo

Shelf architectures of an isolated Late Cretaceous carbonate platform margin, Galala Mountains (Eastern Desert, Egypt)

C. Scheibner[a,*], A.M. Marzouk[b,1], J. Kuss[a]

[a]*Universität Bremen, FB5, P.O. Box 330440, 28334 Bremen, Germany*
[b]*Geology Department, Faculty of Science, Tanta University, Tanta 31527, Egypt*

Received 5 July 2000; accepted 19 April 2001

Abstract

An asymmetrical carbonate platform margin to basin transect has been investigated in the Upper Campanian–Maastrichtian succession of the Galala Mountains, northern Egypt. Identification of systems tracts and their lateral correlation was possible in slope sections only, whereas the monotonous chalk-marl alternations of the basinal sections could not be subdivided with respect to sequence stratigraphic terminology.

The platform asymmetry is expressed by varying large-scale depositional architectures exhibiting a rimmed platform with a sigmoidal slope curvature in south-easterly dip-sections and a ramp with a linear slope curvature in south-westerly dip-sections. The rimmed platform is subdivided into a gentle upper slope and a steep lower slope. The platform formed as a result of the initial topography that was controlled by the tectonic uplift of the Northern Galala/Wadi Araba Syrian Arc structure. The calculated angles of the steep lower slope of the rimmed part range from 5 to 8°, whereas the ramp part has an angle of less than 0.1°.

Keywords: Galala Mountains; Eastern Desert; Egypt; Campanian; Maastrichtian; Asymmetrical carbonate platform; Slope angles; Sedimentary sequences; Sea-level changes; Biostratigraphy

1. Introduction

Carbonate platforms can be differentiated into rimmed platforms and ramps. Rimmed carbonate platforms are marked by a pronounced increase in slope, whereas ramps have a gently sloping depositional surface (generally $<1°$) that passes gradually offshore, with no slope break (Burchette and Wright, 1992). The terms rimmed platform and ramp not only describe the morphology of the slope but normally also imply the biology involved. Rimmed platforms are in most cases associated with 'steep-sloped reefs', whereas ramps are characterised by their absence. If the inherited biology plays a minor role for description of slopes and the focus is more on the morphology or clinoforms, one can more generally speak of linear, exponential and sigmoidal slope profiles (Adams et al., 1998; Adams and Schlager, 2000). The majority of the slope profiles in the literature have a sigmoidal slope curvature, possible reasons for this can be found in Adams et al. (1998) and Adams and Schlager (2000).

During the Campanian–Maastrichtian of the Galala Mountains, Eastern Desert, Egypt, an isolated carbonate platform developed locally on top of an elongated,

* Corresponding author. Fax: +49-421-2184515.
E-mail addresses: scheibne@uni-bremen.de (C. Scheibner), kuss@uni-bremen.de (J. Kuss).
[1] Fax: +2-40-3350804.

0037-0738/01/$ - see front matter
PII: S0037-0738(01)00114-2

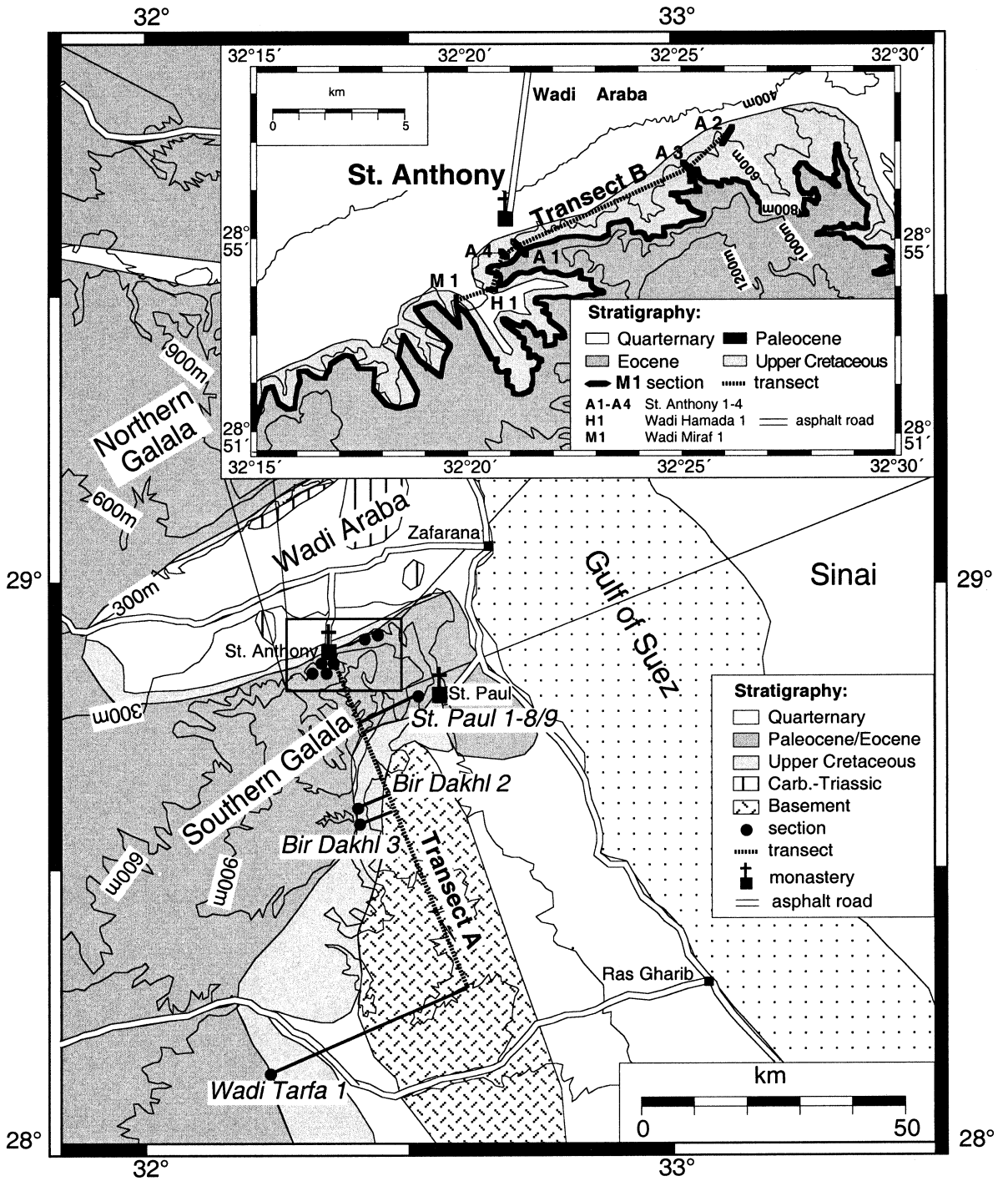

Fig. 1. Schematic geologic map of the northern part of the Gulf of Suez with locations of sections attributing to Transect A (main map) and Transect B (inlay). The sections St Anthony 1, St Paul 9, Bir Dakhl 2–3 and Wadi Tarfa 1 of Transect A are projected on a NNW–SSE running line. Sections Wadi Miraf 1, Wadi Hamada 1 and St Anthony 1–4 of Transect B (see upper inlay for detailed location) are oriented in WSW–ENE direction parallel to the northern escarpment of the Southern Galala.

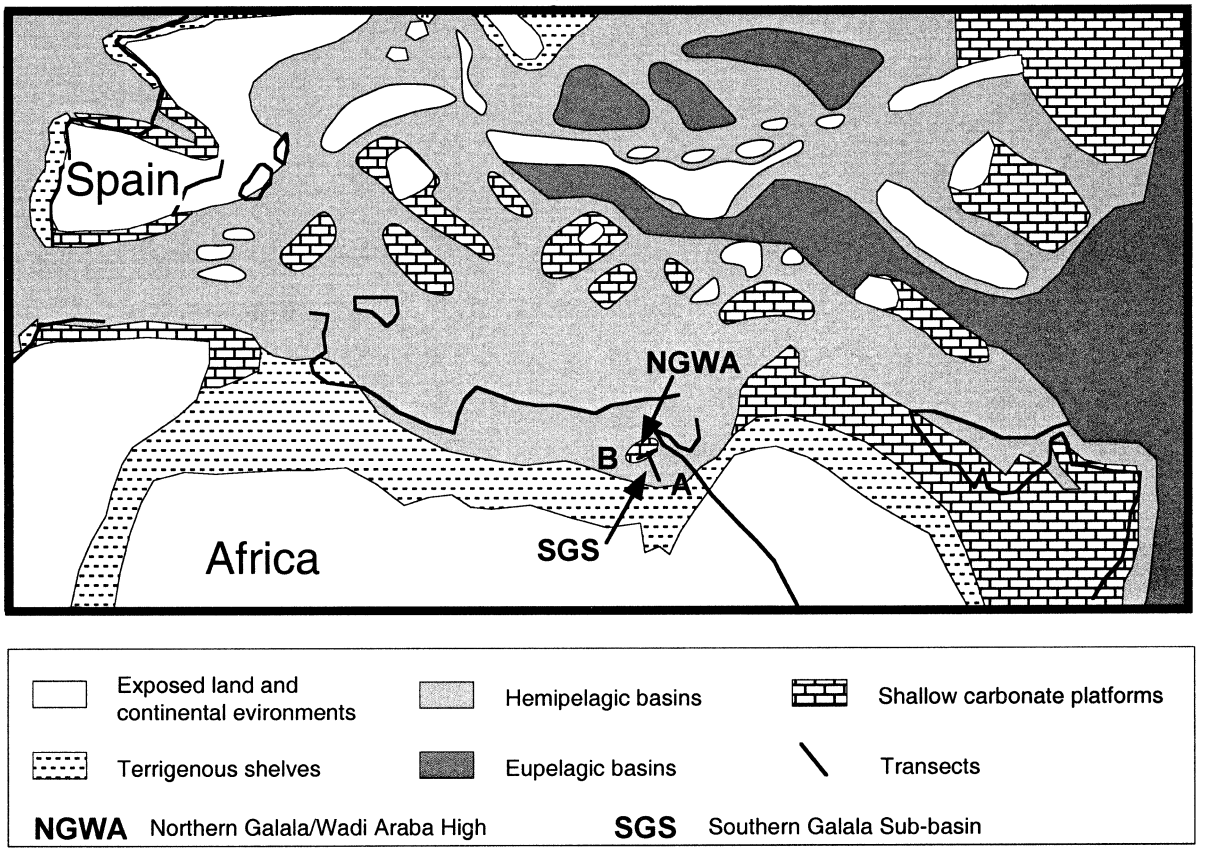

Fig. 2. Late Campanian palaeogeography of the central Tethys (modified from Camoin et al., 1993) with the location of the Northern Galala/Wadi Araba High and the Southern Galala Sub-basin.

tectonically induced WSW–ENE striking Syrian Arc uplift (Moustafa and Khalil, 1995) (Figs. 1 and 2). In this study, we focus on the description and discussion of two platform margin architecture models for this area. As most parts of the carbonate platform were deposited at the locality of today's Wadi Araba (Fig. 1), we can infer information on the depositional history only from the distal parts of the carbonate platform (Kuss et al., 2000; Scheibner et al., 2001.). In these and in other publications (Kuss and Leppig, 1989; Kulbrok, 1996) the terms rimmed platform and ramp were used, although, the terms sigmoidal and linear slope profile are probably more appropriate because the ecological evidence for a rimmed platform is lacking.

Sedimentological and micropalaeontological studies are presented for two transects oriented parallel and perpendicular to the strike of the carbonate platform. Calculations are conducted for the varying degrees of inclination of the slope types of a rimmed carbonate platform model and an asymmetrical carbonate platform model. The latter is formed like a rimmed carbonate platform with a sigmoidal slope curvature in south-easterly directions, but like a ramp with a linear slope curvature in south-westerly directions.

2. Material and methods

The study area extends from the northern rim of the Southern Galala approximately 70 km southwards to Wadi Tarfa (Fig. 1). We investigated in detail 11

Campanian–Maastrichtian sections in two transects: Transect A has a roughly N–S direction with the sections St Anthony, St Paul 9, Bir Dakhl 2–3 and Wadi Tarfa 1. Transect B is oriented in SW–NE direction along the northern rim of the Southern Galala with the sections Wadi Miraf 1, Wadi Hamada 1 and St Anthony 1–4 (Figs. 1 and 2).

Facies and sequence stratigraphic interpretations are based on fine-scale mapping of stratigraphic sections in and along the Northern Galala/Wadi Araba High. Microscopic studies of 66 thin-sections of the Campanian–Maastrichtian interval are supplemented by analyses of 176 washed samples that formed the base for a high-resolution biostratigraphic frame mainly based on calcareous nanoplankton, supplemented by planktic and benthic foraminifera and some macrofossils. These facies and stratigraphic interpretations (Sections 5 and 6) were used as basic parameters for the development of the two platform models (Section 7).

3. Geological setting

Since Turonian times, the area of the Galala Mountains was influenced by vertical movements of the Syrian Arc fold belt, marking the initial stages of the collision between the African and European plates (Moustafa and Khalil, 1995). As a consequence, in northern Egypt and Sinai a system of inverted, uplifted and folded grabens was formed along the Syrian Arc in Egypt also known as the 'unstable shelf' (Said, 1962). In contrast to Syrian Arc Structures on Sinai like Minsherah, Magharah, Hallal, Yelleq and Areif el Naqa (Lüning et al., 1998; Kuss et al., 2001), on top of which basinal deposits were deposited during late Campanian to Palaeogene times, a carbonate platform evolved on the uprising Syrian Arc structure of Northern Galala/Wadi Araba High (Fig. 2). As a consequence of the uplift of the Northern Galala/Wadi Araba High, the Southern Galala Sub-basin evolved further south, forming a part of the Eastern Desert Intrashelf Basin (Kuss et al., 2000).

The Late Cretaceous transition between the Northern Galala/Wadi Araba High and the Southern Galala Sub-basin roughly coincides with the boundary between deformed and undeformed middle-upper Campanian strata and is well exposed along the northern scarp of the Southern Galala Plateau (e.g. near St Anthony, Fig. 1; see also Bandel and Kuss, 1987). At this locality, a major angular unconformity separates steeply south-dipping Turonian–lower Campanian units of the Northern Galala/Wadi Araba High from moderately south-dipping to nearly flat lying upper Campanian–Maastrichtian to lower Eocene strata further south (Southern Galala Sub-basin). Stratigraphic evidence of a long-term elevation in the north (Northern Galala/Wadi Araba High) is illustrated by stratigraphic gaps spanning the Coniacian to late Palaeocene (Kuss et al., 2000; Scheibner et al., 2001). The WSW–ENE striking Northern Galala/Wadi Araba High strongly influenced Cretaceous–Palaeocene sedimentation processes in the studied area. This contains a gently south-dipping carbonate platform, rimming the Northern Galala/Wadi Araba High in the north and interfingering with slope sediments and hemipelagic deposits to the south. In addition, the siliciclastics that were shed from the platform can be explained by this structural element. During the uplift of the Northern Galala/Wadi Araba High, successively older sediments were exposed and subsequently eroded (Bandel and Kuss, 1987). Based on Kulbrok (1996), three major southward prograding carbonate platform systems with different large-scale sedimentary architectures can be distinguished:

- a late Campanian/Maastrichtian rimmed shelf;
- a Palaeocene distally steepened ramp;
- an early Eocene homoclinal ramp.

In this paper, we concentrate on the late Campanian/Maastrichtian rimmed shelf, whereas Scheibner et al. (2000), Kuss et al. (2000) and Scheibner et al. (2001) further discuss the Palaeocene platform development.

4. Lithostratigraphy

The studied late Campanian–Maastrichtian sediments of the Southern Galala area (Fig. 3) consist of deposits of the shallow-water St Anthony Formation

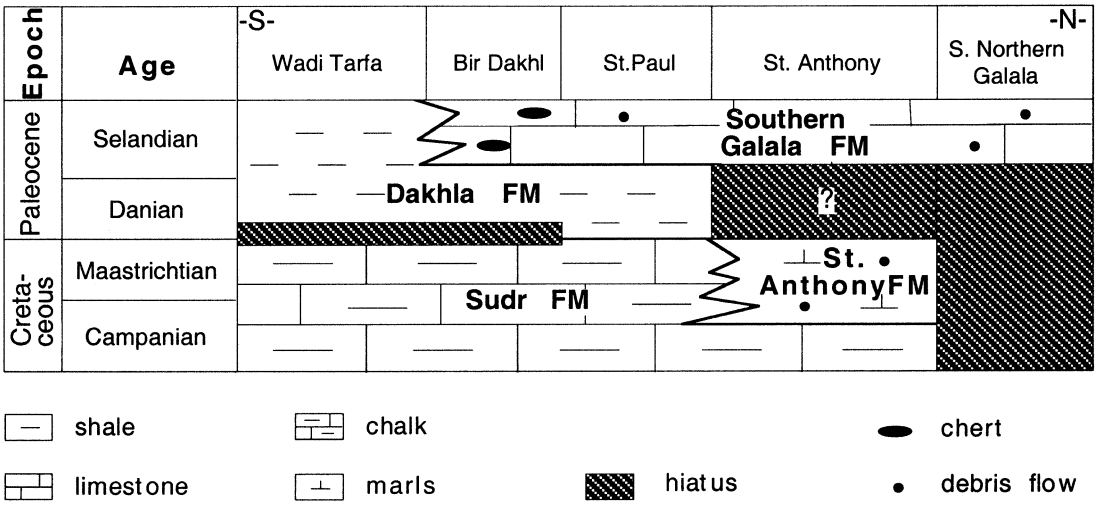

Fig. 3. The late Campanian–Palaeocene formations of the Galala Mountains to illustrate lithofacies changes throughout the working area.

(Transect B) and of deposits of the deep-water Sudr and Dakhla Formations (Transect A) (Figs. 3 and 4). The St. Anthony Formation, predominantly carbonates with slumping features and reworked shallow water biota, disconformably overlies basinal chalks of the Sudr Formation in the northern areas and underlies the carbonates of the Southern Galala Formation. The Sudr Formation consists of massive white and cream coloured chalk and chalky limestone beds with thin intercalations of light greyish calcareous shales and is overlain in the southern areas (Wadi Tarfa-St Paul) by the Dakhla Formation. The Maastrichtian part of the Dakhla Formation consists of chalky marls. A more detailed description and discussion of the biostratigraphic ranges of various Late Cretaceous–Palaeocene formations in the northern Gulf of Suez region will be found in Scheibner et al. (2001).

5. Biostratigraphy

The subdivision of calcareous nanoplankton biozonation into CC-zones was first established by Sissingh (1977). Comparison of the subdivisions of Norris et al. (1998) and Hardenbol et al. (1998) show clear discrepancies of the order of first and last occurrences of important calcareous nanoplankton taxa (Fig. 5). In our samples, the order of first occurrences and last occurrences of calcareous nanoplankton is similar to that in the subdivision of Norris et al. (1998); therefore, we follow their subdivision, including some marker levels provided by Perch-Nielsen (1985).

For planktic foraminiferal zonation, we follow Caron (1985). Similar to Caron (1985), we identified the *Gansserina gansseri* Zone. Index forms of planktic foraminifera are either rare or are strongly diagenetically altered, especially in Transect B, thus limiting their use for biostratigraphy.

In addition, we use *Exogyra overwegi*, benthic foraminifers (*Omphalocyclus macroporus*/*Pseudomphalocyclus blumenthali*, *Orbitoides* sp.) and ammonites (*Discoscaphites kambysis*, *Saghalinites* sp.) for stratigraphic subdivision in Transect B (Fig. 4). In Transect A, only calcareous nanofossils and planktic foraminifers are used for biostratigraphic correlation. For delineating the Campanian–Maastrichtian boundary and correlating zonal schemes of calcareous nanoplankton and planktic foraminifers, we follow Norris et al. (1998) who correlated this stage boundary with a level in lower CC24 (Fig. 5). The samples of the upper parts of the sections of Transect B allowed only preparation of thin-sections. Therefore, the stratigraphic resolution is lower and often uncertain compared to Transect A. This is evident e.g. for the hiatus across the Maastrichtian–Palaeocene boundary (Scheibner et al., 2001).

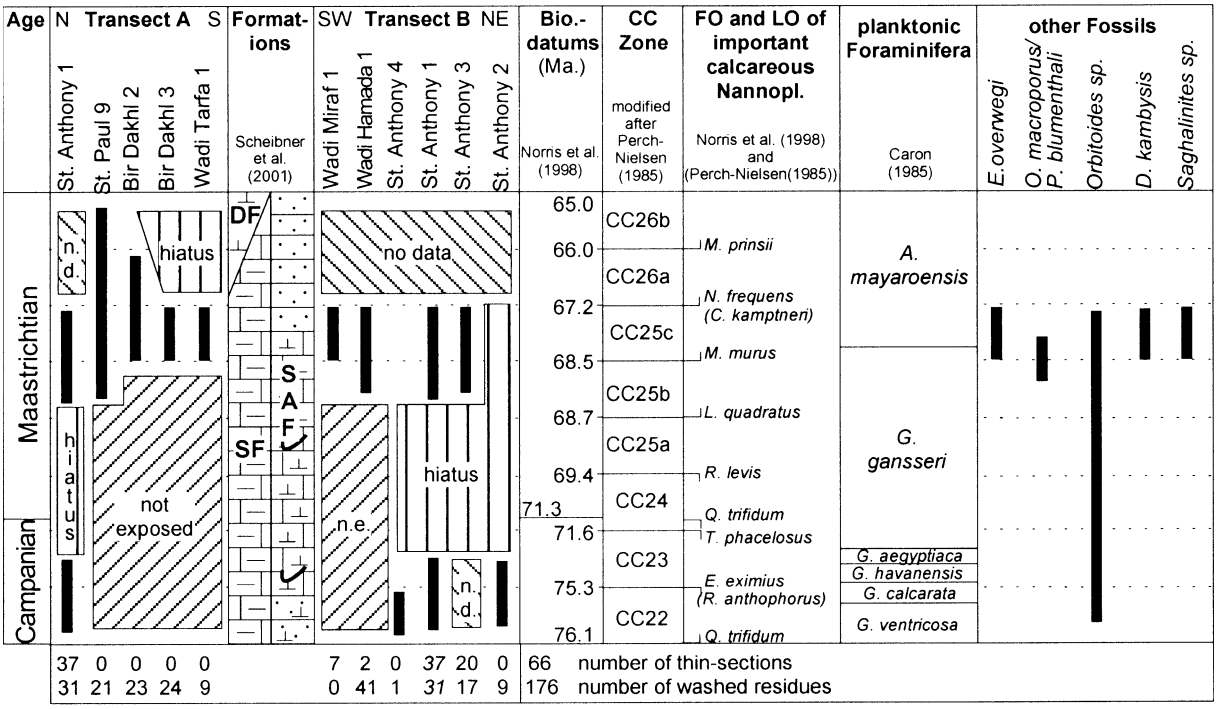

Fig. 4. Stratigraphic ranges of the investigated sections are illustrated in columns 2 and 4 with not exposed (n.e.) lower parts of most sections of Transect A and of sections Wadi Miraf 1 and Wadi Hamada 1 of Transect B. Hiatuses occur in all St Anthony sections, and missing of samples (no data; n.d.) or missing of biostratigraphic subdivision occur in the upper part of all sections in Transect B. Formation names of column 3 refer to a classification given by Scheibner et al. (2001), with chalks of the Sudr Formation (SF) and marls of the Dakhla Formation (DF) occurring in Transect A and chalky limestones, marls and sandstones of the St Anthony Formation (SAF) in all sections of Transect B (for signatures see Fig. 7). The last column gives the stratigraphic ranges of some other fossil groups: oysters (*E. overwegi*); large foraminifers (*Omphalocyclus macroporus/Pseudomphalocyclus blumenthali*, *Orbitoides* sp.); ammonites (*Discoscaphites kambysis*, *Saghalinites* sp.). The number of analysed thin-sections and loose samples (bottom) refer to the respective sections.

6. Sedimentary patterns and systems tracts

6.1. Transect A (Fig. 7)

This ca. 70 km long transect is a projection of the sections onto a line oriented perpendicular to the strike (ENE/WSW) of the carbonate platform with section St Anthony 1 at the northern rim of the Southern Galala and section Wadi Tarfa 1 in the Wadi Tarfa area (Figs. 1 and 7). A schematic sequence of stratigraphic cross-section of Transect A for the Campanian to lower Eocene can be seen in Fig. 6. In the southern basinal sections of Transect A, chalk-marl alternations of the Sudr Formation (composed of up to 120 cm thick chalk-beds and up to 10 cm thick marls) prevail (Figs. 3, 7 and 8k). In section St Paul 9, they range from CC25b to CC26b, whereas in section Wadi Tarfa 1 only CC25c is present. In sections St Paul 9 and Bir Dakhl 2, the upper parts of the Maastrichtian with alternating chalky marl beds are transitional in lithology to the overlying marls and have been partly attributed to the Dakhla Formation (Scheibner et al., 2001). Benthic foraminifera assemblages in section St Paul 9 suggest a bathymetric environment of 300–500 m (R.P. Speijer, personal communication). However, in section St Paul 9, an anomalous 43 cm thick marly, bivalve-rich layer with a neritic (−200 m) benthic foraminifera assemblage has been intercalated in upper CC25b (R.P. Speijer, personal communication). With the exception of section St Anthony 1, a subdivision in systems tracts is not possible. Because of its similarity to the other sections of Transect B, section St Anthony 1 will be described in Section 6.2.

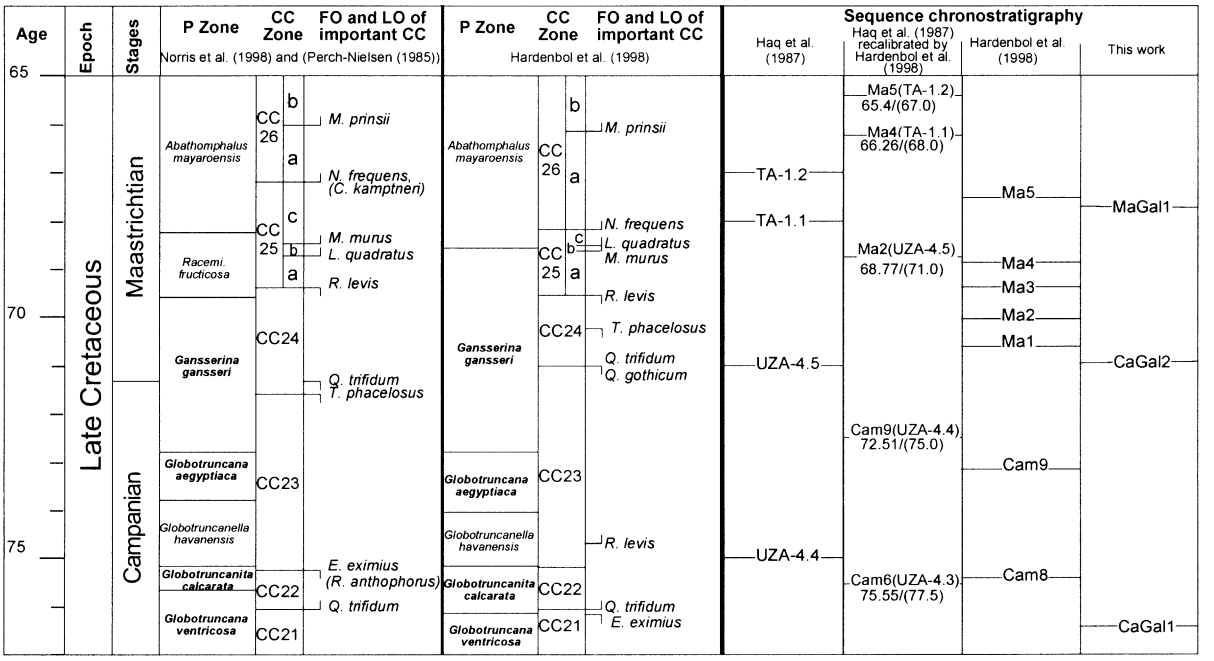

Fig. 5. Biostratigraphy and sequence chronostratigraphy. The two biostratigraphic schemes of Norris et al. (1998)/Perch-Nielsen (1985) and Hardenbol et al. (1998) show various discrepancies of the timing of first occurrence and last occurrence of calcareous nanoplankton. In the sequence chronostratigraphic columns the sequences of Haq et al. (1987) and their recalibration by Hardenbol et al. (1998) are shown. The last column shows sequence boundaries of the Galala Mountains and their biostratigraphic position (calibrated after Norris et al., 1998).

6.2. Transect B

Transect B is oriented parallel to the strike (WSW/ENE) of the carbonate platform along the northern rim of the Southern Galala, measuring about 13 km (Figs. 1 and 9). The system tracts described below are mainly inferred from section St Anthony 1 (Figs. 8a,b and 9) with additional data from the neighbouring sections of Transect B. For the Cretaceous we have found three sequences, CaGal1, CaGal2 and MaGal1. Sequence names are derived from a combination of the stage and the region (Galala), and relate to the underlying sequence boundaries (e.g. sequence CaGal2 is located between sequence boundary CaGal2, below and sequence boundary MaGal1, above).

6.2.1. Sequence CaGal1

Kulbrok (1996) described a sequence boundary (UC1) in St Anthony 3 m below the topmost chalks of the Campanian Sudr Formation at the base of a 0.5 m thick layer with siliciclastic, phosphatic pebbles, corresponding to CaGal1 of Kuss et al. (2000). Lowstand systems tracts (LST) sediments above are characterised by silt- to sandstones and alternations of limestones and silty marls. In the upper part large-scale synsedimentary slumps with dipping directions towards the west are observed in section St Anthony 4 (Fig. 8e,f). The sample below these large slumps indicates CC22. Kulbrok (1996) described *O. gruenbachensis* from these layers. Time-equivalent sediments are found only in section St Anthony 2, composed of hard and soft marly limestones. Due to the monotonous lithology throughout section St Anthony 2 and the poor biostratigraphic resolution, a subdivision into systems tracts is very uncertain. Only the unit with large slumping structures and channel fills around 70 m (Fig. 9) may correlate to the large synsedimentary slumpings of section St Anthony 4 and therefore may be attributed to the LST-deposits of CaGal1 as well.

The following transgressive systems tract (TST) is best exposed in section St Anthony 1, composed of alternating marls and carbonaceous siltstones

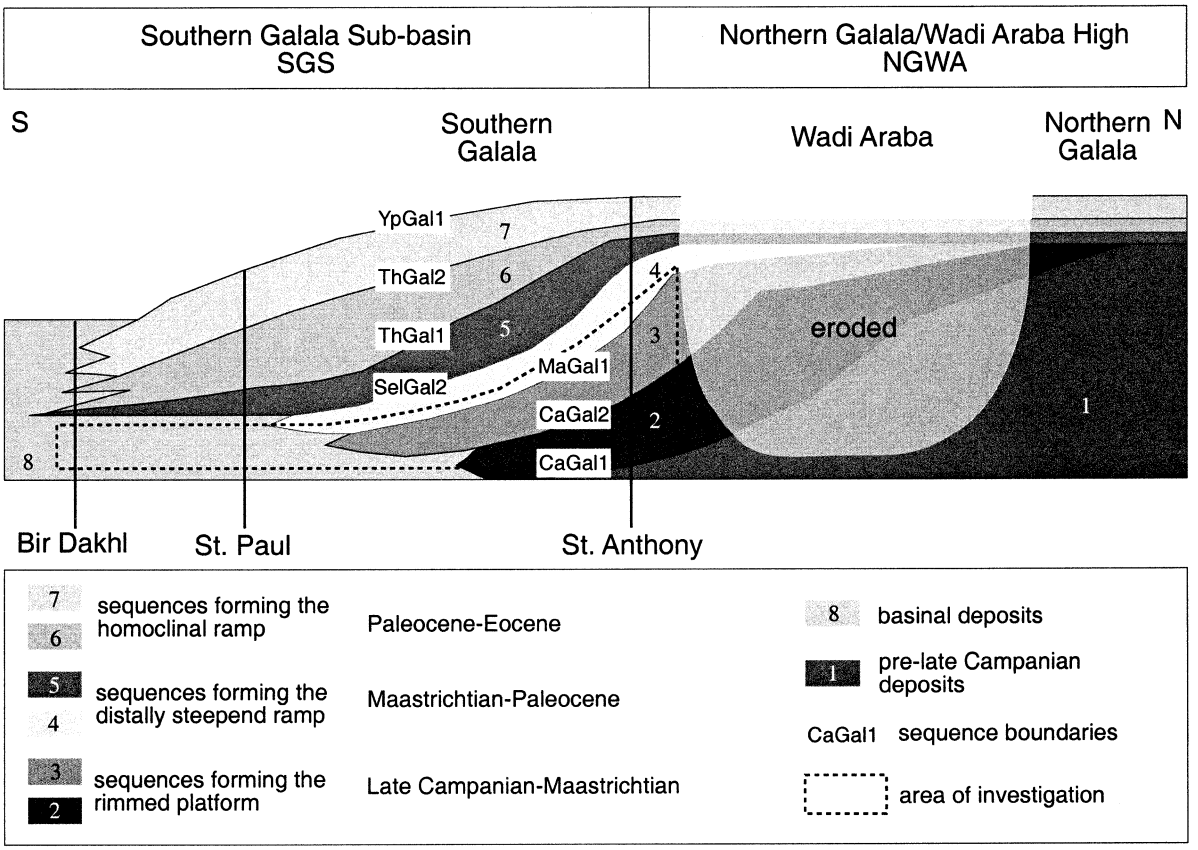

Fig. 6. Schematic cross-section for the late Cretaceous–Palaeocene sedimentary sequences to demonstrate the stratigraphic evolution of three carbonate platforms at the Northern Galala/Wadi Araba High: (2/3) the rimmed carbonate platform, (4/5) the distally steepened ramp; (6/7) the homoclinal ramp. Modified after Kuss et al. (2000).

(between 110 and 155 m of section St Anthony 1; Kulbrok, 1996). The TST and overlying highstand systems tracts (HST) sediments could not be biostratigraphically assigned. However, in section St Anthony 2, the sediments overlying the LST-slumps of CaGal1 can be attributed to CC22 or CC23. Therefore, we assume a similar age of the TST and the HST for both sections St Anthony 1 and St Anthony 2. The HST-deposits of section St Anthony 1 are composed of bioclastic limestones with abundant fragments of coralline algae and shells. The top of the HST is characterised by a 0.15 m thick silty sandstone and a 0.5 m thick limestone, both with rare to abundant *Exogyra* sp.

The top of this hard limestone layer marks the sequence boundary CaGal2 (Fig. 9). We correlate the base of the debris flow in section St Anthony 2 (around 140 m, Fig. 9) with sequence boundary CaGal2. However, we cannot substantiate this correlation through independent biostratigraphic data.

6.2.2. Sequence CaGal2

The sediments of the CaGal2-LST can be attributed to CC25b due to the presence of *L. quadratus*. In none of the sections, CC24 or CC25a was encountered; therefore, we assume a stratigraphic gap for that interval coinciding with sequence boundary CaGal2 (Fig. 9).

Similar to the CaGal1-LST, the CaGal2-LST is composed of marls and limestones with a subordinate siliciclastic content. Conspicuous synsedimentary slumpings occur. The top of the LST-deposits is characterised in section St Anthony 1 by

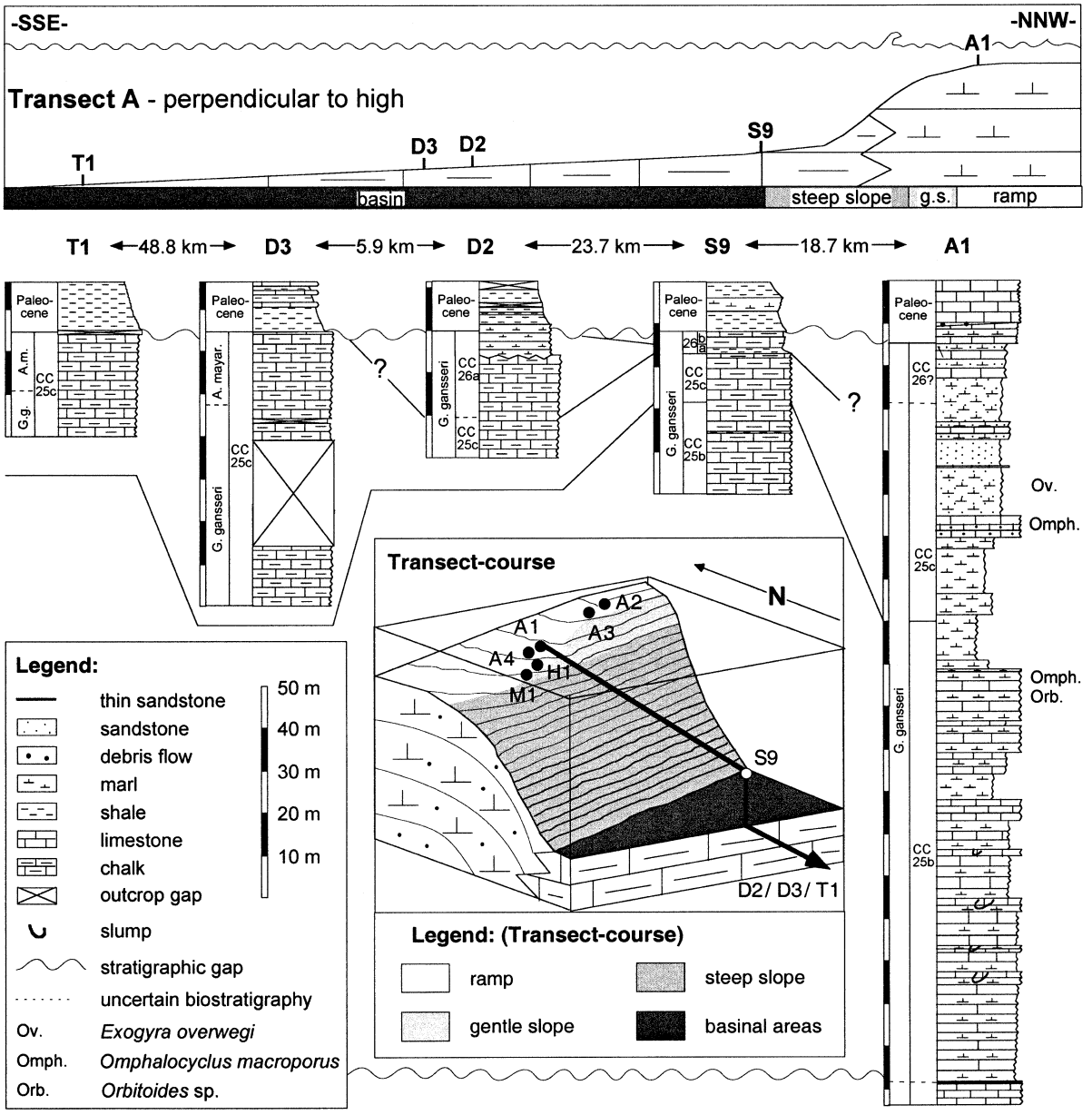

Fig. 7. Litho- and bio-stratigraphic correlation of the five sections along Transect A (Fig. 1); the lower 160 m of section St Anthony 1 are illustrated in Fig. 9. The mainly basinal chalks prevent a subdivision into systems tracts. The position of the 2D transect (top) is indicated in a 3D graph (bottom). The grey shades in the 2D and 3D graphs indicate the simplified morphology of the Maastrichtian platform margin. (T1 = Wadi Tarfa1; D2/3 = Bir Dakhl 2/3; S9 = St Paul 9; A1 = St Anthony 1).

bioclastic limestones with *O. macroporus* and/or *P. blumenthali* and in section St Anthony 3 by a slumped limestone bed (1.40 m) with abundant bivalves, gastropods and corals.

The TST starts in sections Wadi Hamada 1 and St Anthony 1 in the upper part of CC25b and in section St Anthony 3 at the top of CC25b (Fig. 9), and is composed of alternating hard and soft

yellow marls with a high planktic foraminiferal content (50–75%). In section Wadi Hamada 1, only the middle to upper TST-sediments are exposed, compared with age-equivalent deposits of the neighbouring section St Anthony 1 (Fig. 9). Further to the ENE, in sections St Anthony 3 and St Anthony 2, the stratigraphic range of the TST decreases (demonstrated by the different position of the CC25b/CC25c boundary). The lateral variations can be explained either by diachroneity of the TST-deposits ('eastward onlapping') or by laterally changing sedimentation-rates.

The overlying HST is characterised either by mass flow deposits (Wadi Hamada 1) or by conglomeratic, partly bedded marls to limestones with moderate siliciclastic contents (Wadi Miraf 1, St Anthony 1, St Anthony 3). Increasing thicknesses of the conglomeratic/mass flow units are evident from ENE (St Anthony 3) to WSW (Wadi Miraf 1) indicating a low angle gradient towards the west. *O. macroporus* and/or *P. blumenthali* and Lepidorbitoididae (*Praesiderolithes douvillei*?), coralline algae, gastropods and echinodermata are obvious in the HST deposits of sections Wadi Miraf 1, St Anthony 1, St Anthony 3. Abundant *Thalassinoides* burrows, the shallow water bivalve *Pinna*, and teeth of bony fishes, that thrived in calm-water-zones of reefs (C. Werner, personal communication) were found in section St Anthony 3. The top of the carbonaceous mass flow unit coincides with sequence boundary MaGal1. Only in the westernmost section Wadi Miraf 1, 2.7 m thick dolomitic marls occur on top of the mass flow unit underlying sequence boundary MaGal1.

6.2.3. Sequence MaGal1

This sequence starts in all sections with the first *E. overwegi* beds (Fig. 8d,g). It overlies in section St Anthony 2 mass flow deposits and underlies Palaeocene limestones on top (Fig. 9). In all other sections (St Anthony 3, St Anthony 1, and Wadi Miraf 1) the MaGal1-LST-sediments exhibit a clear three-fold lithologic subdivision: the reddish to yellowish siliciclastic marls at the base hold distinct layers of *E. overwegi*, *Exogyra* sp., other bivalves, gastropods (Fig. 8c) and bioturbations (Fig. 8i). Internally, this unit is characterised by shallowing-up cycles of thick layers with siliciclastic marls without bivalves and by thin layers with bivalves. These shallowing-up cycles (Fig. 8h) are best visible in section St Anthony 3, whereas in sections St Anthony 1 and Wadi Miraf 1, the molluscous layers are less frequent and the carbonate content increases indicating again a low angle depth gradient towards the west. The middle parts of the LST contain similar sediments except for the absence of *E. overwegi*; again, an increase of the carbonate content from ENE to WSW is evident. In section St Anthony 3, the shallowing-up cycles are emphasised by colour contrasts of red and white, where white marks the shallower bioturbated parts (Fig. 8h,i). In section St Anthony 3, the upper parts of the LST are characterised by sandstones, whereas in sections St Anthony 1 and Wadi Miraf 1, hard and soft marls and limestones alternate.

Fig. 8. (a,b) Photograph and sketch of the mainly Maastrichtian–Palaeocene deposits of section St Anthony 1 with the two sequence boundaries CaGal2 and MaGal1. The encircled letters indicate the stratigraphic position (not always the location) of the appropriate photographs (c–e,g,j) from different sections. Best visible are the huge LST-deposits of sequence CaGal2. The MaGal1 LST-deposits are illustrated in detail in (g). The steep cliff on top marks the Palaeocene. Compare signatures of the systems tracts to Fig. 9. (c) Accumulation of turritellid gastropods in the LST-deposits of sequence MaGal1 (section St Anthony 1), stratigraphic position is indicated in (g). (d) Sandy limestones with *Exogyra overwegi* in the HST-deposits of sequence CaGal2 (section St Anthony 1), stratigraphic position is indicated in (g). (e,f) Photograph and sketch of the synsedimentary slumpings in LST-deposits of sequence CaGal1 (section St Anthony 4). GP represents a mayor gliding plane of the slumpings that are visible in distorted bedding planes further west. (g) The MaGal1 LST-deposits in section St Anthony 3 (Fig. 1). The encircled letters indicate the position of (c,d,h,i). The steep cliff on top represents Palaeocene limestones. (h) Shallowing-up cycle within the MaGal1 LST-deposits in section St Anthony 3. The lower massive part is characterised by red siliciclastic marls with a concentration of shells (1). The upper thin part is build of white, calcareous bioturbations (Fig. 1). (i) Top view onto the white calcareous bioturbations of a shallowing-up cycle in the LST-deposits of MaGal 1 in section St Anthony 3 (detail of h). (j) Marly TST-deposits of CaGal2 in section Wadi Hamada 1 yielding the best-preserved calcareous nanoplankton and planktonic foraminifera in Transect B. The steep cliff is build of the conglomeratic carbonates of the HST-deposits of CaGal2. (k) Late Maastrichtian monotonous chalk-marl alternations of the Sudr Formation in section Bir Dakhl 2.

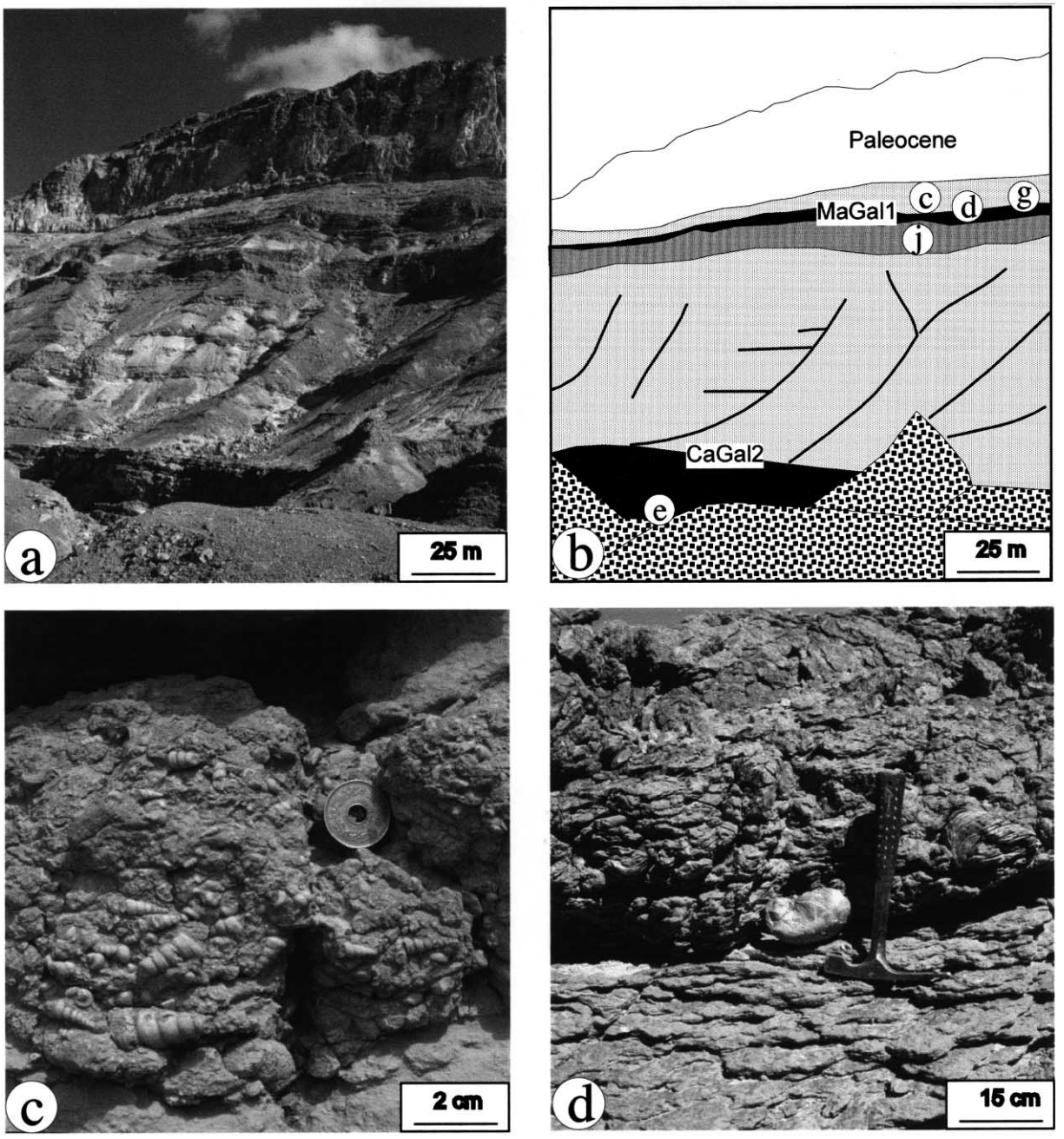

7. Carbonate platform morphology

The sedimentary patterns of the Late Campanian–Maastrichtian carbonate platform margin sediments of the Galala Mountains can be explained by two principal platform models reflecting two different platform architectures (Fig. 10):

- A: a rimmed carbonate platform with a W–E strike-direction (straight), A′: a rimmed

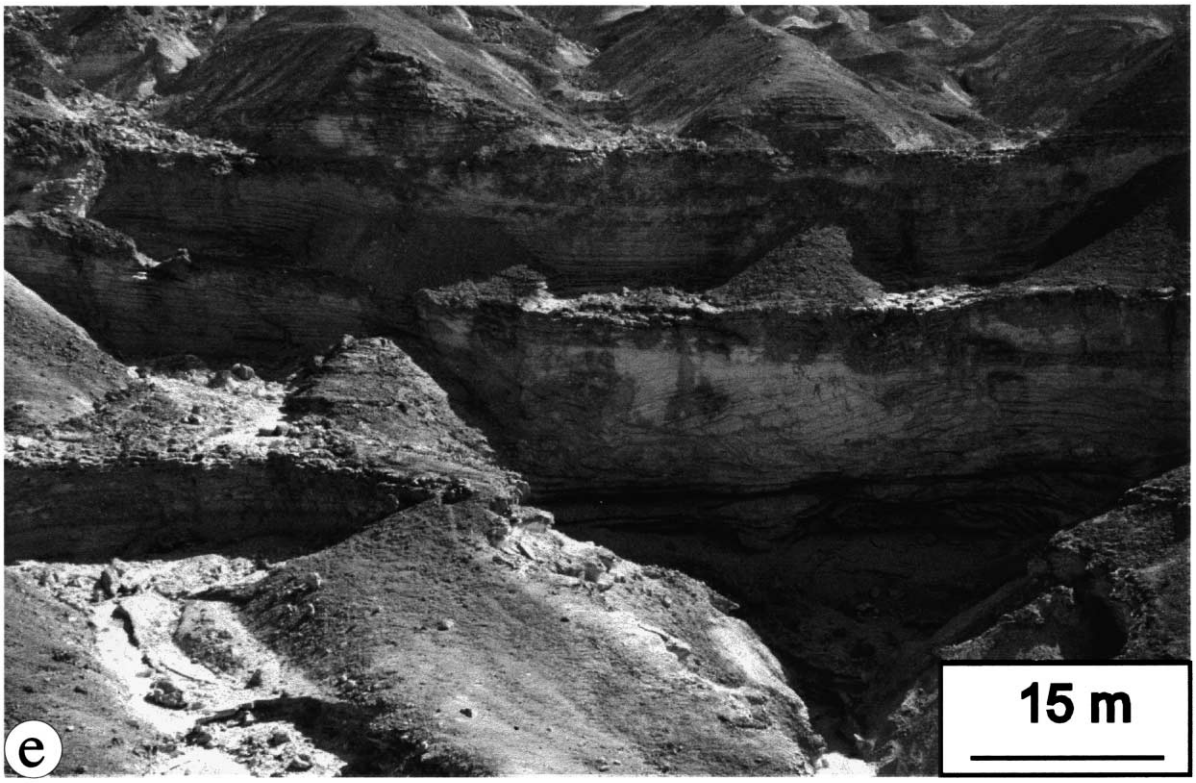

Fig. 8. (*continued*)

carbonate platform with a ENE–WSW strike (oblique model) both with sigmoidal slope profiles and

- B: an asymmetrical carbonate platform with a gently W-dipping ramp part with a linear slope profile and a WSW–ENE striking rimmed part, also with a sigmoidal slope profile (Fig. 10).

7.1. Model parameter

The rimmed part with the sigmoidal slope profile of both models A/A′ and B can be separated into two

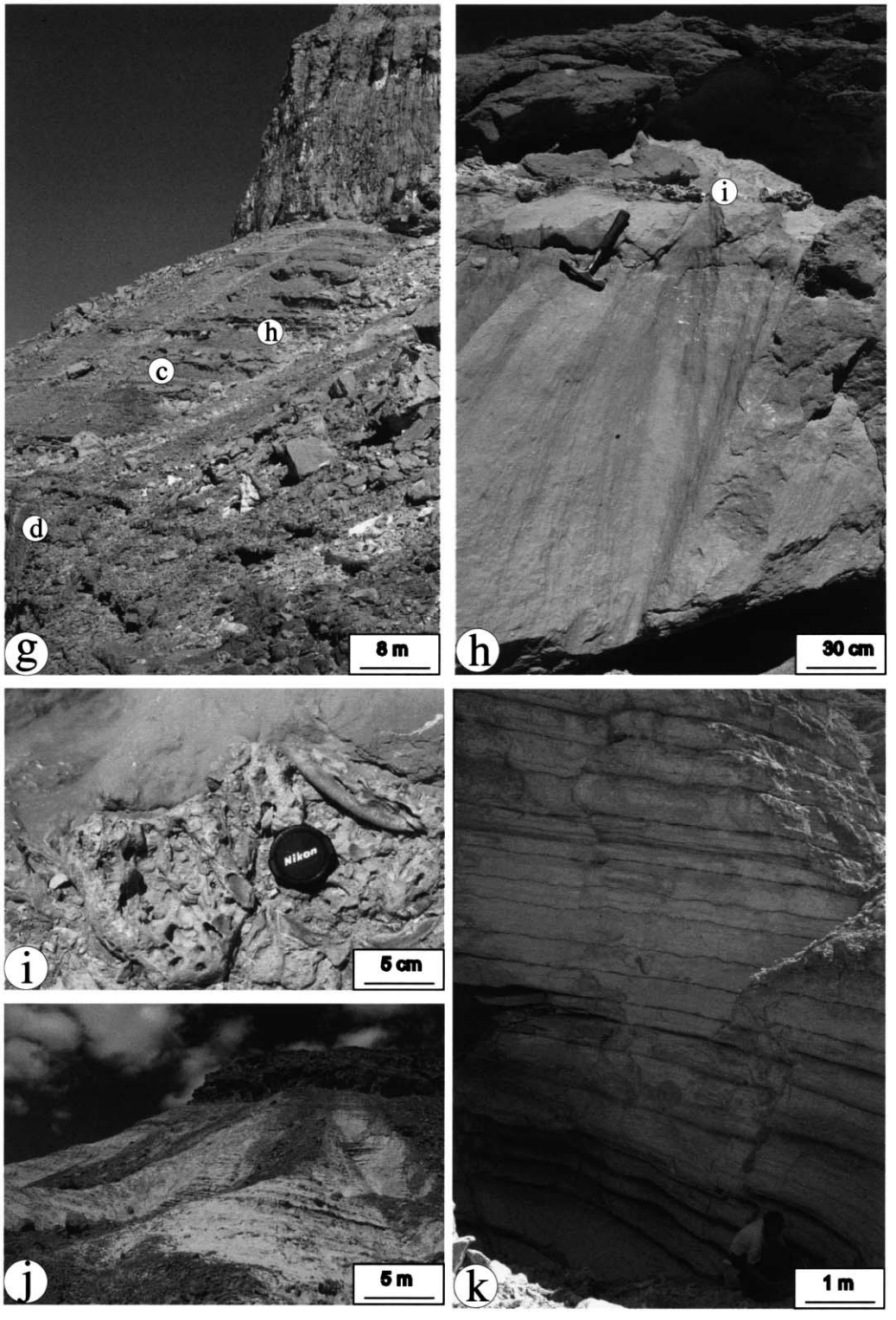

Fig. 8. (*continued*)

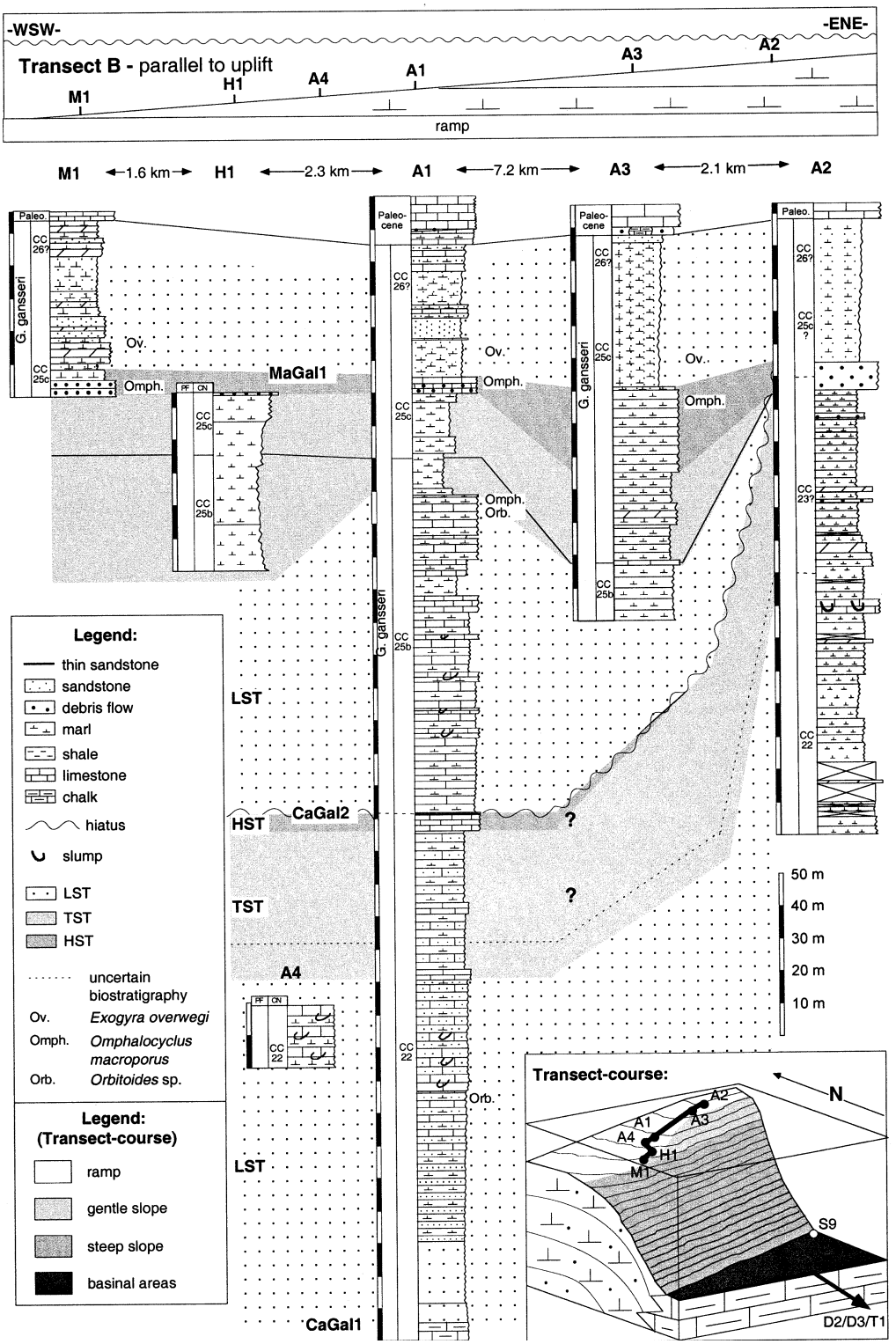
-WSW-
-ENE-
Transect B - parallel to uplift
M1
H1
A4
A1
A3
A2
ramp
M1 ←1.6 km→ H1 ←2.3 km→ A1 ←7.2 km→ A3 ←2.1 km→ A2
Paleo.
Paleo-cene
G. gansseri
CC 26?
CC 25c
CC 25b
CC 23?
CC 22
Ov.
Omph.
Orb.
MaGal1
CaGal2
CaGal1
LST
TST
HST
A4
PF
CN
?
50 m
40 m
30 m
20 m
10 m
Legend:
thin sandstone
sandstone
debris flow
marl
shale
limestone
chalk
hiatus
slump
LST
TST
HST
uncertain biostratigraphy
Ov. Exogyra overwegi
Omph. Omphalocyclus macroporus
Orb. Orbitoides sp.
Legend: (Transect-course)
ramp
gentle slope
steep slope
basinal areas
Transect-course:
N
A2
A1
A3
A4
H1
M1
S9
D2/D3/T1

differently inclined slopes, an upper gentle slope and a lower steep slope. If not using this bipartition, the angle of the entire slope would be significantly higher and thus would lead to larger depth-differences between the sections in Transect B, which is not supported by the sedimentary patterns. For the following calculations, the hinge-line between the gentle slope and the steep slope has been chosen close to section Wadi Miraf 1, whereas the transition from the steep slope to the basinal parts varies.

For both models, we assume a palaeowater-depth for section St Anthony 2 (East) of 70 m and for section Wadi Hamada 1 (West) of 90 m; both assumptions are based on palaeoecologic interpretations of benthic foraminifera assemblages in biozones CC25b and CC25c (K. Schnack, personal communication). The difference in palaeowater-depths between both sections is confirmed by sedimentary patterns (synsedimentary slumpings with a gliding plane dipping in westerly directions, more pronounced shallowing-up cycles in the easterly sections and increasing debris-flow depths in westerly directions) and palaeoecologic data (findings of shallow-water biota and burrows in section St Anthony 3), which hint to shallower water-depths in easterly directions. For the calculation of the angle of inclination, the following formula has been used (Fig. 10):

$$\tan a = \mathrm{WD}/(D \times 1000)$$

with: a = angle of inclination, WD = water depth (m), D = distance (km)

7.1.1. Models A/A′

The rimmed carbonate platform model with a sigmoidal slope curvature assumes that the palaeowater-depths of sections Wadi Miraf 1, Wadi Hamada 1, St Anthony 4, St Anthony 1, St Anthony 3 and St Anthony 2 (Transect B) were oriented in ascending order on a proximal part of the slope (Fig. 10) while sections St Paul 9, Bir Dakhl 2, Bir Dakhl 3 and Wadi Tarfa 1 represent the distal, basinal parts (Transect A). The strike of the slope could be oriented either in W–E direction (straight model A) or in WSW/ENE direction (oblique model A′). In both situations, the slope is subdivided into a gentle and a steep part (Fig. 10). The degree of inclination of the gentle slope varies from 0.15° (model A) to 0.38° (model A′). Calculations are based on a palaeowater-depth difference of 20 m between sections St Anthony 2 and Wadi Miraf 1 and the distance between both (perpendicular to the direction of the slope). The degree of inclination of the steep slope varies between 3.1 and 8.5° (model A) and between 1.3 and 8.5° (model A′). For section St Paul 9, we assume a water-depth of about 400 m (the benthic foraminifers assemblages suggest water-depths of 300–500 m; R. P. Speijer, personal communication), hence the water-depth difference between sections Wadi Miraf 1 and St Paul 9 is about 300 m.

The most critical difference between the two basic models A and A′ concerns the position of the slope-basin transition. Because we do not know, whether the water-depth of 400 m is reached exactly at section St Paul 9 or further north, we calculated the inclinations of the slope with various distances (Table 1). By choosing a maximum distance of 5.5 km (model A) or 13 km (model A′) and a palaeowater-depth difference of 300 m, the inclination of the steep slope would vary between 3.1° (model A) and 1.3° (model A′). A reduction of the distance between section Wadi Miraf 1 and the slope-basin-transition would result in a steepening of the slope (for a 2 km distance, the inclination would rise up to 8.5°) (Table 1).

7.1.2. Model B

In this model, we assume an asymmetrical carbonate platform, with a gently WSW dipping ramp with a linear slope profile and a WNW–ESE striking rimmed carbonate platform with a sigmoidal slope profile (Fig. 10). Transect B traverses the ramp part and Transect A traverses the rimmed carbonate platform part. For the ramp part, we calculate an angle of inclination of 0.08°, based on assumptions of a 20 m of water-depth difference and a distance of 15 km (St Anthony 2–Wadi Miraf 1; measured perpendicular to the isobathes). For the gentle slope and the steep slope of the rimmed carbonate platform part, we assume the

Fig. 9. Sequence-stratigraphic correlation of the six sections of Transect B. The position of the 2D transect (top) is indicated in a 3D graph (bottom). The grey shades in the 2D and 3D graphs indicate the simplified morphology of the Maastrichtian platform margin. (M1 = Wadi Miraf 1; H1 = Wadi Hamada 1; A1–4 = St Anthony 1–4).

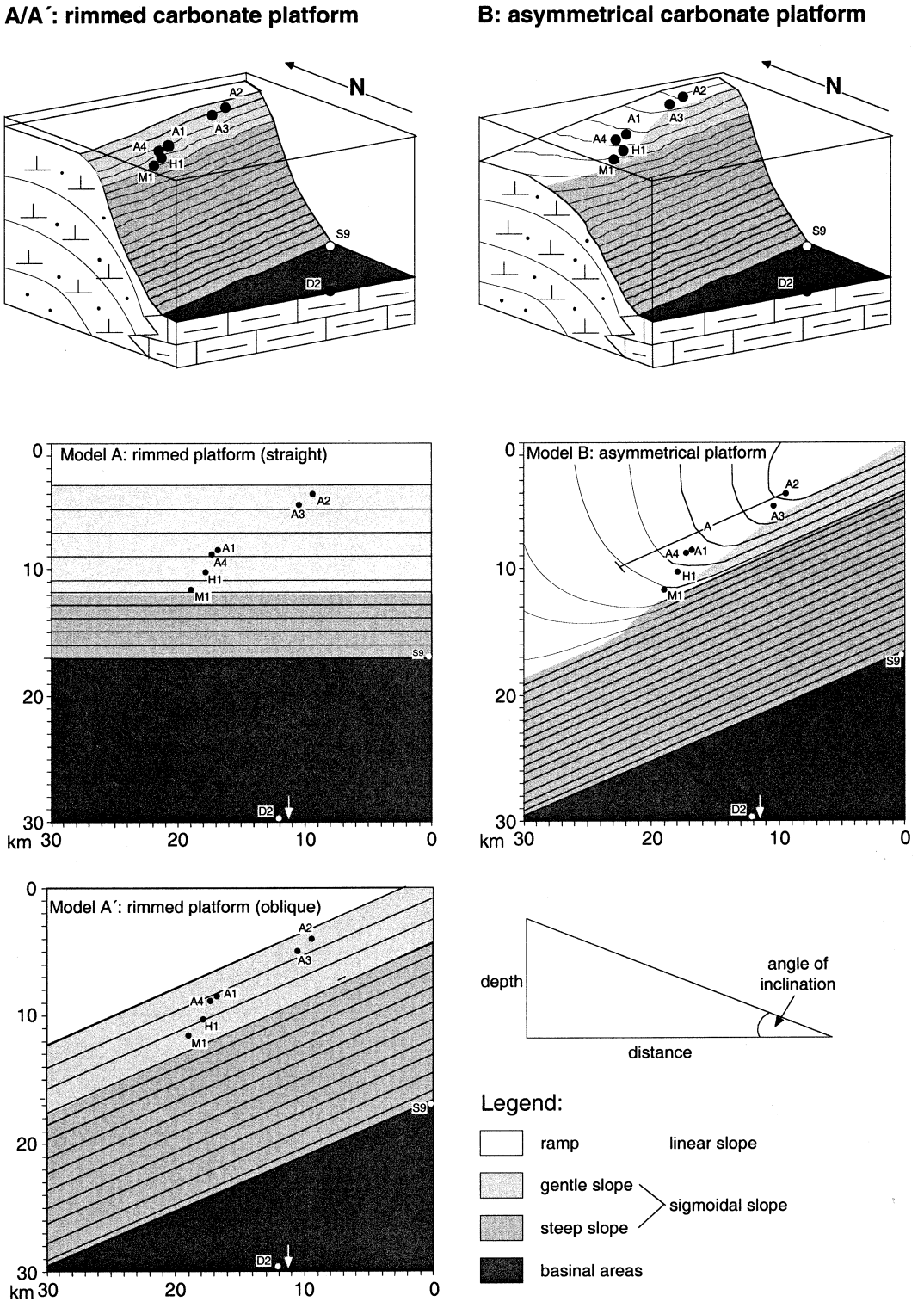
A/A´: rimmed carbonate platform
B: asymmetrical carbonate platform
N
A2
A3
A1
A4
H1
M1
S9
D2
Model A: rimmed platform (straight)
Model B: asymmetrical platform
Model A´: rimmed platform (oblique)
A
0
10
20
30
km 30
20
10
0
depth
angle of inclination
distance
Legend:
ramp
linear slope
gentle slope
steep slope
sigmoidal slope
basinal areas

same angles of inclination as for the gentle and steep parts of the rimmed carbonate platform of model A′ (Table 1). The inclination of the steep slope would also increase, if the slope-basin transition and the gentle slope–steep slope hinge-line would be closer to each other.

8. Discussion

8.1. Correlation of sequences and sea-level changes

The correlation of our sedimentary sequences is based on biostratigraphic correlations that may cause confusion when using the Haq et al. (1987) sea-level curve. We do not refer to the general points of criticism (e.g. Miall 1992, 1997) but to the chronologies involved. The new sequence chronostratigraphic chart of Hardenbol et al. (1998) includes a recalibration of the earlier Haq et al. (1987) record (Fig. 5). With this recalibration, the old sequence boundaries of Haq et al. (1987) shifted approximately 2 my upward (younger) so that e.g. the often cited sea-level fall at 71 Ma (Miller et al., 1999; Li et al., 1999) now has an age of 68.77 Ma (Hardenbol et al., 1998), and hence could not be correlated with the sea-level fall around 71 Ma (Miller et al., 1999; Li et al., 1999).

In our sections of Transect B, a hiatus spans biochrones CC24 to CC25a with a total duration of at least 3 million years from 72 to 69 Ma (after Norris et al., 1998; Fig. 5). Assuming a 40 m sea-level fall around 71 Ma (Miller et al., 1999) which is in the lower part of CC24 (Norris et al., 1998), a subaerial exposure of the sediments in our sections is not realistic: no sedimentologic evidence of exposure is visible, and the benthic foraminifera assemblages of the post-hiatus sediments suggest a water-depth of about 100 m that would be far more than the amount of the proposed sea-level fall and subsequent rise. If the hiatus around 71 Ma in our sections is attributed to an eustatic sea-level fall, it remains uncertain which processes led to the non-deposition and/or erosion. Possible reasons can be changed water circulation or bottom currents, condensed sections attributed to subsequent rise of sea-level or gravitational transport mechanisms like slumpings which led to the observed hiatus. In combination with eustatic sea-level changes, tectonic uplift of the Northern Galala/Wadi Araba High may have resulted in the observed hiatus. A similar hiatus was reported by Li et al. (1999) from age-equivalent sediments of Tunisia.

The sea-level fall at MaGal1 also could be the result of a eustatic sea-level fall as Haq et al. (1987) and Li et al. (1999) recorded a sea-level fall around 68 Ma. But local tectonic uplift movements of the Northern Galala/Wadi Araba High could not be ruled out because of the sudden high siliciclastic content of the whole sequence that should have their source somewhere farther north in the main regions of the Northern Galala/Wadi Araba High.

8.2. Carbonate platform models

All the three models require a deepening from NE (section St Anthony 3) to SW (section Wadi Miraf 1). This deepening can be demonstrated below and above sequence boundary MaGal1 by sedimentologic parameters like increasing carbonate contents from NE to SW, increasing thicknesses of the mass flow units from NE to SW (due to larger accommodation spaces) and in an emphasis of the shallow-up cycles in the NE section St Anthony 3. Palaeoecologic parameters like findings of shallow-water dwellers e.g. *Pinna* sp. and of teeth of bony fishes (preferring reefal environments) in calcareous nanoplankton zones CC25 of section St Anthony 3 (NE) also suggest a shallowing towards NE. Kulbrok (1996) described sections

Fig. 10. Comparison of different carbonate/siliciclastic platform-margin architectures based on two 3D models and their respective top views. Location of the sections along Transect A and B are taken from GPS readings and refer to a km-grid with isobathes to illustrate different palaeo-inclinations. Models A and A′ show a rimmed carbonate platform with a sigmoidal slope curvature which strike in E–W and WSW–ENE directions. Model B is an asymmetrical carbonate platform with a WSW–ENE striking rimmed carbonate platform and additionally a gentle W-dipping ramp with a linear slope curvature. Section Bir Dakhl 2 lies farther south, the southernmost sections Bir Dakhl 3 and Wadi Tarfa 1 (Fig. 1) are not indicated. Within the three models a ramp part, a gentle slope and a steep slope can be distinguished based on different inclinations. Calculation of geometric relations, resulting in these different inclinations is given in Table 1.

Table 1
Calculation of the angle of inclination for the different parts of the platform-margin and for various water-depth differences. For the calculation of the angle of inclination, the following formula has been used: tan a = WD/($D \times 1000$) with a = angle of inclination, WD = water depth (m), D = distance (km). For all calculations, a water-depth of 70 m for St Anthony 2 and of 90 m for Wadi Miraf 1 is assumed. In models A and A′ the gentle slope between sections St Anthony 2 and Wadi Miraf 1 (direction measured perpendicular to the slope) vary from 0.152° (model A) to 0.382° (model A′). The steep slope of models A and A′ are calculated with different water-depth between sections Wadi Miraf 1 and St Paul 9 and different distances from Wadi Miraf 1 to the point of the slope-basin transition. The bold characters below the number 300 (difference in water-depth between sections Wadi Miraf 1 and St Paul 9, in m) indicate the probable angles of inclination. The smaller the distance between Wadi Miraf 1 and the slope-basin transition, the steeper the slope. The ramp part of the asymmetrical carbonate platform model B has an inclination of 0.076°, whereas the gentle and the steep slope of the rimmed carbonate platform part have the same angles as the corresponding angles of the rimmed carbonate platform of model A′. The different distances between sections St Anthony 2 and Wadi Miraf 1 is due to the fact that these distances were measured perpendicular to the isobathes

Model A: rimmed platform (straight)
Gentle slope

Water depth A2	70 m
Distance from A2–M1 (N–S)	7.5 km
Water-depth M1	90 m
Angle of inclination	0.152°

Steep slope

		Difference in water depth between M1 and S9 (m)								
Distance from M1 to Water-depth (N–S, in km)		100.00	150.00	200.00	250.00	**300.00**	350.00	400.00	450.00	500.00
WD	5.5	1.04	1.56	2.08	2.60	**3.12**	3.64	4.16	4.68	5.19
	5.0	1.15	1.72	2.29	2.86	**3.43**	4.00	4.57	5.14	5.71
	4.5	1.27	1.91	2.54	3.18	**3.81**	4.45	5.08	5.71	6.34
	4.0	1.43	2.15	2.86	3.58	**4.29**	5.00	5.71	6.42	7.13
	3.5	1.64	2.45	3.27	4.09	**4.90**	5.71	6.52	7.33	8.13
	3.0	1.91	2.86	3.81	4.76	**5.71**	6.65	7.59	8.53	9.46
	2.5	2.29	3.43	4.57	5.71	**6.84**	7.97	9.09	10.20	11.31
	2.0	2.86	4.29	5.71	7.13	**8.63**	9.93	11.31	12.68	14.04

Results = α, angle of inclination (°)

farther in the west with depositional settings deeper than that of section St Anthony 1. The only direct evidence for a palaeoslope not only dipping in SE directions but also in SW directions comes from the large synsedimentary slumpings visible in section St Anthony 4 of biozone CC22 (Fig. 8e,f). Their gliding planes are dipping roughly E–W and thus require a palaeoslope that is also oriented in E–W direction. These architecture requirements would fit with model B.

Other evidence for model B concerns the underlying structure. Many Syrian Arc structures on Sinai like Minsherah, Magharah, Hallal, Yelleq or Areif el Naqa (Moustafa and Khalil, 1995; Lüning et al., 1998a,b; Kuss et al., 2001) exhibit double plunging anticlines, generally striking in ENE–WSW directions. Steep flanks are dipping in SE direction and gentle flanks in SW direction. This applied to the Syrian Arc Northern Galala/Wadi Araba High, representing the structural unit underneath the Late Cretaceous carbonate platform, supports the asymmetrical carbonate platform model B.

Slope angles in carbonate systems are recorded from less than 1° to up to more than 40° (Read, 1985). According to Kenter (1990), the sediment fabric is a major control on slope angles. Cohesionless sediments, such as clean sands and rubble, build up to angles over 40°, modified by shearing and avalanching. Muddy, cohesive sediments tend to maintain a low slope angle, decreasing to less than 15° for mud-supported fabrics and less than 5° for pure mud, modified by large-scale creep and rotational to translational sliding and slumping (Kenter, 1990).

The sediments of the investigated Upper Cretaceous platform margin are mainly composed of a muddy and mud-supported fabric with large-scale slumping, similar to those of the middle Miocene of the Little Bahama Bank (Kenter, 1990), where slope

Table 1 (*continued*)

Model A′: rimmed platform (oblique)										
Gentle slope										
Water-depth A2	70 m									
Distance from A2–M1 (NW–SE)	3 km									
Water-depth M1	90 m									
Angle of inclination	0.382°									
Steep slope										
		Difference in water-depth between M1 and S9 (m)								
Distance from M1 to Water-depth (NW–SE, in km)		100.00	150.00	200.00	250.00	**300.00**	350.00	400.00	450.00	500.00
WD	13.0	0.44	0.66	0.88	1.10	**1.32**	1.54	1.76	1.98	2.20
	12.5	0.46	0.69	0.92	1.15	**1.37**	1.60	1.83	2.06	2.29
	12.0	0.48	0.72	0.95	1.19	**1.43**	1.67	1.91	2.15	2.39
	11.5	0.50	0.75	1.00	1.25	**1.49**	1.74	1.99	2.24	2.49
	11.0	0.52	0.78	1.04	1.30	**1.56**	1.82	2.08	2.34	2.60
	10.5	0.55	0.82	1.09	1.36	**1.64**	1.91	2.18	2.45	2.73
	10.0	0.57	0.86	1.15	1.43	**1.72**	2.00	2.29	2.58	2.86
	9.5	0.60	0.90	1.21	1.51	**1.81**	2.11	2.41	2.71	3.01
	9.0	0.64	0.95	1.27	1.59	**1.91**	2.23	2.54	2.86	3.18
	8.5	0.67	1.01	1.35	1.68	**2.02**	2.36	2.69	3.03	3.37
	8.0	0.72	1.07	1.43	1.79	**2.15**	2.51	2.86	3.22	3.58
	7.5	0.76	1.15	1.53	1.91	**2.29**	2.67	3.05	3.43	3.81
	7.0	0.82	1.23	1.64	2.05	**2.45**	2.86	3.27	3.68	4.09
	6.5	0.88	1.32	1.76	2.20	**2.64**	3.08	3.52	3.96	4.40
	6.0	0.95	1.43	1.91	2.39	**2.86**	3.34	3.81	4.29	4.76
	5.5	1.04	1.56	2.08	2.60	**3.12**	3.64	4.16	4.66	5.19
	5.0	1.15	1.72	2.29	2.86	**3.43**	4.00	4.57	5.14	5.71
	4.5	1.27	1.91	2.54	3.18	**3.81**	4.45	5.08	5.71	6.34
	4.0	1.43	2.15	2.86	3.58	**4.29**	5.00	5.71	6.42	7.13
	3.5	1.64	2.45	3.27	4.09	**4.90**	5.71	6.52	7.33	8.13
	3.0	1.91	2.86	3.81	4.76	**5.71**	6.65	7.59	8.53	9.46
	2.5	2.29	3.43	4.57	5.71	**6.84**	7.97	9.09	10.20	11.31
	2.0	2.86	4.29	5.71	7.13	**8.53**	9.93	11.31	12.68	14.04
Results = α, angle of inclination (°)										
Model B: asymmetrical platform										
Ramp part										
Water-depth A2	70 m									
Distance from A2-M1	15 km									
Water-depth A2	90 m									
Angle of inclination	0.076°									
Gentle slope										
Same as the gentle slope of model A′										
Steep slope										
Same as the steep slope of model A′										

angles vary between 2 and 4°. As this example ranges at the lower end of the range spectrum for muddy to mud-supported sediments given by Kenter (1990), we would expect little higher values for the inclination of the Upper Cretaceous slope. Values of 5–8° were calculated for all three models with the combination of the following parameters: a 300 m difference in water-depth between section

Wadi Miraf 1 and section St Paul 9 and a 2–3 km distance between the hinge-line of the gentle/steep slope and the transition between steep slope and basin (Fig. 10; Table 1).

9. Conclusions

System tracts could only be identified in the slope sections of Transect B, while the monotonous chalk-marl alternations of the basinal sections of Transect A could not be subdivided. The identified sea-level changes of sequences CaGal1, CaGal2 and MaGal1 are at least partly of eustatic origin but a tectonic component could not be ruled out, especially for the long lasting hiatus at sequence boundary CaGal2 and for the enhanced siliciclastic input of sequence MaGal1 a tectonic contribution may explain part of the sea-level changes.

We calculated the slope geometries referred to two principal carbonate platform models (rimmed platform, asymmetrical platform). Because of the initial structural topography and sedimentary patterns, the model of an asymmetrical platform is favoured. This asymmetrical platform margin is formed like a rimmed platform with a sigmoidal slope profile in south-easterly direction and like a ramp with a linear slope profile in south-westerly direction. The rimmed platform can be subdivided into a gentle upper slope and a steep lower slope. The palaeowater-depth between the slope sections and the basinal sections change from 100 m (slope) to 300–500 m in the basinal sections. These differences in water-depth lead to angles of the steep slope of the rimmed part of 5–8°, whereas the ramp part would have an angle of less than 0.1°.

Acknowledgements

A.M. Bassiouni (Ain Shams University) is especially thanked for many logistic supports. A.M. Morsi (Ain Shams University) is thanked for his open ear for all problems encountered during our stay in Egypt. R.P. Speijer (University of Bremen) is thanked for comments on the previous version of this paper. We thank J.A.M. Kenter, T. Aigner and B. Sellwood for their reviews and suggestions for improving the manuscript. A. Scharf, R. Bätzel and M. Brinkmann (all from University of Bremen) aided with sample preparation. The investigations were funded by the Graduiertenkolleg 'Stoff-Flüsse in marinen Geosystemen' of the University of Bremen and the German Science Foundation (DFG).

References

Adams, E.W., Schlager, W., 2000. Basic types of submarine slope curvature. J. Sedim. Res. 70, 814–828.

Adams, E.W., Schlager, W., Wattel, E., 1998. Submarine slopes with an exponential curvature. Sedim. Geol. 117, 135–141.

Bandel, K., Kuss, J., 1987. Depositional environment of the pre-rift sediments — Galala Heights (Gulf of Suez, Egypt). Berliner geowiss. Abh. A 78, 1–48.

Burchette, T.P., Wright, V.P., 1992. Carbonate ramp depositional systems. Sedim. Geol. 79, 3–57.

Camoin, G., Bellion, Y., Dercourt, J., Guiraud, R., Lucas, J., Poisson, A., Ricou, L.E., Vielrynck, B., 1993. Late Maastrichtian Palaeoenvironments (69.5–65). In: Dercourt, J., Ricou, L.E., Vrielynck, B. (Eds.), Atlas Tethyan Palaeoenvironmental Maps. BEICIP-FRANLAP, Rueil-Malmaison.

Caron, M., 1985. Cretaceous planktic foraminifera. In: Bolli, H.M., Saunders, J.B., Perch-Nielsen, K. (Eds.), Plankton Stratigraphy. Cambridge University Press, Cambridge, pp. 17–86.

Haq, B.U., Hardenbol, J., Vail, P., 1987. Chronology of fluctuating sea levels since the triassic. Science 235, 1156–1167.

Hardenbol, J., Thierry, H., Farley, M.B., Jacquin, T., De Graciansky, P., Vail, P.R., 1998. Mesozoic and Cenozoic sequence chronostratigraphic framework of European basins. In: de Graciansky, P.C., Hardenbol, J., Jacquin, T., Vail, P.R. (Eds.), Mesozoic and Cenozoic Sequence Stratigraphy of European Basins. SEPM, Tulsa, pp. 3–13.

Kenter, J.A.M., 1990. Carbonate flanks: slope angles and sediment fabric. Sedimentology 37, 777–794.

Kuss, J., Scheibner, C., Gietl, R., 2000. Carbonate platform to basin transition along an Upper Cretaceous to Lower Tertiary Syrian arc uplift, Galala Plateaus, Eastern Desert, Egypt. Geoarabia 5, 405–424.

Kuss, J., Westerhold, T., Groß, U., Bauer, J., Lüning, S., 2001. Mapping of Late Cretaceous stratigraphic sequences along a Syrian arc uplift — examples from the Areif el Naqa/Eastern Sinai. Middle East Research Center, in press.

Li, L., Keller, G., Stinnesbeck, W., 1999. The Late Campanian and Maastrichtian in northwestern Tunisia: palaeoenvironmental inferences from lithology, macrofauna and benthic foraminifera. Cretac. Res. 20, 231–252.

Lüning, S., Kuss, J., Bachmann, M., Marzouk, A.M., Morsi, A.M., 1998a. Sedimentary response to basin inversion: Mid Cretaceous–Early Tertiary pre- to syn- deformational deposition at the Areif El Naqa Anticline (Sinai, Egypt). Facies 38, 103–136.

Lüning, D., Marzouk, A.M., Kuss, J., 1998b. Sequence stratigraphy of the Upper Cretaceous of central east Sinai, Egypt. Cretac. Res. 19, 153–196.

Miall, A.D., 1992. Exxon global cycle chart: an event for every occasion? Geology 20, 787–790.

Miall, A.D., 1997. The Geology of Stratigraphic Sequences. Springer, Berlin.

Miller, K.G., Barrera, E., Olsson, R.K., Sugarman, P.J., Savin, S.M., 1999. Does ice drive early Maastrichtian eustasy? Geology 27, 783–786.

Moustafa, A.R., Khalil, M.H., 1995. Superposed deformation in the northern Suez Rift, Egypt: relevance to hydrocarbons exploration. J. Petrol. Geol. 18, 245–266.

Norris, R.D., Kroon, D., Klaus, A., 1998. Explanatory notes. Proceedings of the Ocean Drilling Program Initial Reports, vol. 171B, pp. 11–44.

Perch-Nielsen, K., 1985. Mesozoic calcareous nannofossils. In: Bolli, H.M., Saunders, J.B., Perch-Nielsen, K. (Eds.), Plankton Stratigraphy. Cambridge University Press, Cambridge, pp. 329–426.

Read, J.F., 1985. Carbonate platform facies models. AAPG Bull. 69, 1–21.

Said, R., 1962. The Geology of Egypt. Elsevier, Amsterdam.

Scheibner, C., Kuss, J., Marzouk, A.M., 2000. Slope sediments of a Palaeocene ramp-to-basin transition in NE Egypt. Int. J. Earth Sci. 88, 708–724.

Scheibner, C., Marzouk, A.M., Kuss, J., 2001. Maastrichtian–Early Eocene lithostratigraphy and palaeogeography of the N Gulf of Suez Region, Egypt. J. Afr. Earth Sci. 32 in press.

Sissingh, W., 1977. Biostratigaphy of Cretaceous nanoplankton. Geol. Mijnbouw 56, 37–65.